Research in Astronomy and Astrophysics, 23:125009 (10pp), 2023 December https://doi.org/10.1088/1674-4527/acf1e3

A Study of Elemental Abundance Pattern of the *r*-II Star HD 222925

Fang Wen[1], Wan-Qiang Han[2], Wen-Yuan Cui[1], Hong-Jie Li[3], and Bo Zhang[1]
[1] College of Physics, Hebei Normal University, Shijiazhuang 050024, China; wenyuancui@126.com, cuiwenyuan@hebtu.edu.cn, zhangbo@hebtu.edu.cn
[2] Department of Physics, Shijiazhuang University, Shijiazhuang 050035, China
[3] School of Sciences, Hebei University of Science and Technology, Shijiazhuang 050018, China
Received 2023 April 22; revised 2023 June 22; accepted 2023 July 11; published 2023 October 31

Abstract

HD 222925 is a rare *r*-process enhanced star in the Milky Way because of its metal abundance ($[Fe/H] = -1.46 \pm 0.10$) and Eu abundance ($[Eu/Fe] = 1.32 \pm 0.08$). Based on the very complete set of elemental abundances of HD 222925, we use the abundance decomposition method to fit the observed abundances of 58 elements in the sample star, which is also the largest number of elemental abundances fitted at the same time for a fixed star. We analyze the astrophysical origins of elements in HD 222925 by its abundance ratios and component ratios. It is found that the light elements and the iron group elements in HD 222925 mainly originate from the primary process of the Type II supernovae (SNe II) with the progenitor mass $M > 10\,M_{\odot}$ and have no contribution from SNe Ia and the first generation of very massive stars. The contribution of the weak *r*-process to Ga, Ge, and As is superior to that of the other processes, and its contribution decreases linearly with increasing atomic number. The main *r*-process that is likely derived from a neutron star merger plays a key role in the formation of neutron-capture elements ($Z \geqslant 38$) in HD 222925.

Key words: stars: chemically peculiar – stars: individual (HD 222925) – nuclear reactions – nucleosynthesis – abundances – stars: abundances

1. Introduction

The slow (*s*-) and the rapid (*r*-) neutron-capture process are thought to be the main mechanisms to produce elements heavier than iron. The *r*-process can be divided into two categories: the weak *r*- and the main *r*-processes. Only light neutron-capture elements can be created by the weak *r*-process that may happen in Type II supernovae (SNe II) with a progenitor mass $M > 10\,M_{\odot}$, while both light and heavy neutron-capture elements can be created by the main *r*-process. Possible astrophysical sites of the main *r*-process that have been suggested are core-collapse supernovae (Buridge & Burbidge 1957; MacFadyen & Woosley 1999; Winteler et al. 2012; Nishimura et al. 2015; Mösta et al. 2018; Fraser & Schönrich 2022) and binary neutron star mergers (NSMs) (Freiburghaus et al. 1999; Goriely 2012; Abbott et al. 2017; Watson et al. 2019; Dvorkin et al. 2021), which is still an open question.

The *r*-process enhanced stars provide important information about the nature of the *r*-process, which can help us to further understand the *r*-process and explore its astrophysical sites. According to the values of [Eu/Fe], the *r*-process enhanced stars can be classified into two groups: the *r*-I stars with $0.3 \leqslant [Eu/Fe] \leqslant 1.0$ and the *r*-II stars with $[Eu/Fe] > 1.0$ (Beers & Christlieb 2005). The abundance patterns of heavy elements with $Z > 56$ of both *r*-I and *r*-II stars are in good agreement with the scaled solar *r*-process pattern, so the *r*-process is a universal nucleosynthesis way (Ivans et al. 2006; Burris et al. 2000; Frebel et al. 2007).

A pure *r*-process signature can only be shown in the *r*-II stars that are not or least affected by the *s*-process (Frebel 2010). Most of the known *r*-II stars usually have very low metallicities with $[Fe/H] < -2.5$ (Sneden et al. 1996; Cayrel et al. 2001; Barklem et al. 2005; Hayek et al. 2009; Li et al. 2015; Ji et al. 2016), while the moderately metal-poor *r*-II stars($-2 < [Fe/H] < -1$) are rare. Only three *r*-II stars with $-2 < [Fe/H] < -1$ have been discovered in the Milky Way so far, HD 222925($[Fe/H] = -1.46$, $[Eu/Fe] = 1.32$), J1802-4404 ($[Fe/H] = -1.55$, $[Eu/Fe] = 1.05$) and 2MASS 18174532-3353235 ($[Fe/H] = -1.67$, $[Eu/Fe] = 0.99$)(Roederer et al. 2018, 2022; Hansen et al. 2018; Johnson et al. 2013). HD 222925 and J1802-4404 are halo stars, while 2MASS 18174532-3353235 is a bulge star. In addition, the moderately metal-poor *r*-II stars are also found in some dwarf galaxies. Shetrone et al. (2001) discovered two *r*-II stars in the Ursa Minor dwarf spheroidal galaxy. One of the two stars, cos 82, has $[Fe/H] = -1.42$ and $[Eu/Fe] = 1.49$ (Aoki et al. 2007), it is similar to HD 222925. Ji et al. (2016) identified a *r*-II star of relatively high-metallicity($[Fe/H] \sim -2$), J033457-540531 with extremely high *r*-process elemental abundances of $[Eu/Fe] \sim 1.7$ when studying the nine brightest known red giants ($-3.5 < [Fe/H] < -2$) in the ultra-faint dwarf galaxy Reticulum II. Considering the moderately metal-poor *r*-II stars ($-2 < [Fe/H] < -1$) having higher metallicities than the other

known *r*-II stars, they are very valuable for a comprehensive understanding of the main *r*-process.

HD 222925 has the highest abundance of Eu ([Eu/H] = −0.14) among all *r*-process enhanced stars known in the Milky Way (Roederer et al. 2018, 2022), so it attracts more attention. Roederer et al. (2018, 2022) determined the abundances of 63 elements in HD 222925 based on the high-resolution optical spectra and ultraviolet (UV) spectra. This abundance set is the most complete for any object beyond the solar system. Investigating the astrophysical origins of the elements in HD 222925 using this abundance set can help us understand the formation of the sample star.

Navarrete et al. (2015) suggested that the enriched Ba in HD 222925 was likely to come from an unseen companion by the mass transfer, which has passed through the asymptotic giant branch (AGB) phase. This means that HD 222925 should have the *s*-process characteristic. However, they did not further verify this. Roederer et al. (2018) pointed out that HD 222925 has no companion by monitoring its radial velocity. Moreover, they suggested that HD 222925 was not affected by the *s*-process by comparing the matching degree between the abundances of elements($Z \geqslant 38$) in HD 222925 and the scaled solar *r*-process residuals. However, the solar *r*-process residuals are not a direct result, and it is obtained by subtracting the *s*-process contribution from the total abundances of the solar system. In this work, we further illustrate the absence of *s*-process characteristics in HD 222925 based on the observed abundances of the sample star and the multiple components model.

In addition, Roederer et al. (2018) concluded that the progenitor system may be similar to the remaining population of ultra-faint dwarf galaxies if the *r*-process material in HD 222925 was derived from a single, high-yield *r*-process event, which might be a neutron star merger. A detailed discussion is needed.

In this paper, how the observed abundances of HD 222925 used for this study were obtained is presented in Section 2. The multiple components model is used to fit the observed abundances of HD 222925 and to speculate the astrophysical origin of elements in Section 3. Using the calculation method from Yang et al. (2017), we analyze the formation of HD 222925 in Section 4. The conclusion is given at the end.

2. Acquisition of Observed Abundances of HD 222925

The sample star HD 222925 is a red horizontal-branch (RHB) field star identified by Gratton et al. (2000). The high-resolution spectra of HD 222925 were obtained using the Magellan Inamori Kyocera Echelle spectrograph (MIKE) in 2018. The spectra were reduced with the CarPy MIKE reduction pipeline (Kelson et al. 2000; Kelson 2003), and processed with the IRAF software by Roederer et al. (2018). Based on the high-resolution optical spectra of the sample star, Roederer et al. (2018) determined the stellar atmospheric parameters and the abundances of 46 elements ($6 \leqslant Z \leqslant 90$) in HD 22925 using MOOG with LTE. They derived [Fe I/H] = −1.56 and [Fe II/H] = −1.47, and the metallicity of HD 222925 was identified as −1.47 when taking the NLTE correction (+0.07) for Fe I lines into account. The enhanced levels of Ba and Eu in HD 22925 were also determined: [Ba/Fe] = 0.55 ± 0.06 and [Eu/Fe] = 1.33 ± 0.08. In 2022, the high-quality ultraviolet (UV) spectroscopy of HD 222925 was obtained by the Space Telescope Imaging Spectrograph on the Hubble Space Telescope, which was coadded and normalized using the IRAF software (Roederer et al. 2022). Adopting the same atmospheric model and stellar parameters as in Roederer et al. (2018), Roederer et al. 2022 derived abundances for 45 elements in HD 222925 using the 404 absorption lines in the UV spectra. They included elements such as Ga, Ge, As, Se, Cd, In, Sn, Sb, Te, W, Re, Pt and Au, which were infrequently tracked in *r*-II stars and not measured in Roederer et al. (2018). By combining the abundance results from optical and UV lines, Roederer et al. (2022) recommended the most complete abundance collection for an extrasolar object, which included 63 elements in HD 222925. In this abundance collection, the abundances of elements with $Z \leqslant 30$ from the optical spectra and UV spectra are consistent, while the abundances of other elements were critically estimated on a case-by-case basis (see Appendix A in Roederer et al. 2022).

According to the recommended elemental abundances of HD 222925 in Roederer et al. (2022), we fit the abundance pattern of 58 elements. The two elements C and N are generally not studied in the multiple components model because in stars the element C may transform into the element N, while the elements P, S and K cannot be studied due to lack of primary component abundances.

3. The Astrophysical Origins of Elements in HD 222925

3.1. Model and Calculations

The chemical elements in stars usually come from the molecular clouds where they were born, and they can be produced through multiple mechanisms. In general, the formation of elements with $Z < 30$ is related to SN explosions, and the neutron-capture elements are produced by the *s*- and /or *r*-process (Woosley & Weaver 1995; Travaglio et al. 2004; Roederer et al. 2010). To study the astrophysical origins of each element in HD 222925, we adopt the multiple components model to fit its observed abundances. The *s*-component abundances are taken from Bisterzo et al. (2010), here we adopt the 1.5 $M_{\odot}$ model at [Fe/H] = −2.0 with ST/12 (see their Table B6), since the calculated ratios [Pb/Ba] = 0.06 is close to the observed ratio [Pb/Ba] = 0.02, and the abundances are normalized to the main *s*-component of Ba abundance in the solar system. The *r*-component abundances of Ge, As, Se,

W and Re are from Niu et al. (2014), Han et al. (2018), Arlandini et al. (1999). Based on the roughly linear relationship between the weak *r*-process contribution to the *r*-process abundances of the solar system and the atomic number (Li et al. 2013), the component abundances of the two *r*-processes for the elements Ga, Cd, In, Sn, Sb, Te and Ta are estimated in this work. The *r*-component abundances of other elements are obtained from Li et al. 2013. The multiple components model is represented as (Han et al. 2020):

$$N_i = (C_{r,m}N_{i,r,m} + C_{\rm pri}N_{i,\rm pri} + C_{s,m}N_{i,s,m} + C_{\rm sec}N_{i,\rm sec} + C_{Ia}N_{i,Ia}) \times 10^{[Fe/H]} \quad (1)$$

where N_i is the abundance of the ith element. $N_{i,r,m}$, $N_{i,\rm pri}$, $N_{i,s,m}$, $N_{i,\rm sec}$ and $N_{i,Ia}$ represent the scaled component abundances of the main *r*-processes, primary process, main *s*-processes, secondary process and SNe Ia, respectively. The component abundances of the primary process contain the abundances of the primary light elements, iron group elements and weak *r*-process elements. On the other hand, the component abundances of the secondary process contain the abundances of the secondary light elements, iron group elements and weak *s*-process elements. $C_{r,m}$, $C_{\rm pri}$, $C_{s,m}$, $C_{\rm sec}$ and C_{Ia} are the corresponding coefficients. To determine the five coefficients in Equation (1), χ^2 is defined as:

$$\chi^2 = \sum_{i=1}^{n} \frac{(\log N_{i,\rm obs} - \log N_{i,\rm cal})^2}{(\triangle \log N_{i,\rm obs})^2 (K - K_{\rm free})} \quad (2)$$

where $\log N_{i,\rm obs}$ and $\triangle \log N_{i,\rm obs}$ are the observed abundance and error of the ith element, which are adopted from Roederer et al. (2022). $\log N_{i,\rm cal}$ is the calculated abundance of the ith element, which can be determined by Equation (1). K and $K_{\rm free}$ are the number of elements studied and the number of free parameters, where K and $K_{\rm free}$ are equal to 58 and 5, respectively.

In the calculation, we obtain the minimum value of χ^2 is 1.71, and five component coefficients are $C_{r,m} = 21.3$, $C_{\rm pri} = 3.3$, $C_{s,m} = 0.5$, $C_{\rm sec} = 0.2$ and $C_{Ia} = 0$. Obviously, $C_{r,m}$ is an order of magnitude larger than $C_{\rm pri}$ and two orders of magnitude larger than $C_{s,m}$ and $C_{\rm sec}$, which suggests that the neutron capture elements in HD 222925 are mainly originated from the main *r*-process and the influence of the *s*-process on HD 222925 is almost negligible. The results indicate that the characteristics of HD 222925 are consistent with those of the *r*-II star. $C_{Ia} = 0$ means that SNe Ia made no contribution to the element abundances of HD 222925. SNe Ia begins to contribute to the interstellar medium at [Fe/H] ~ -1.0 in the Milky Way (Kobayashi et al. 1998), while in dwarf galaxies the contributions of SNe Ia can start at [Fe/H] $\ll -1.0$ (Cohen & Huang 2009; Letarte et al. 2010; Tsujimoto 2011). Based on the metallicity and high [α/Fe]($\sim$0.40) of HD 222925, we speculate that the contribution of SNe Ia should not have been present yet.

We add to Equation (1) the Prompt component, $C_P N_{i,P}$, which may arise from the first generation of very massive stars (Qian & Wasserburg 2001), and refit the observed abundance pattern of HD 222925. Due to the lack of Prompt component abundances for O and Cu, we have studied 56 elements in HD 222925. The calculated results show that $C_{r,m}$, $C_{\rm pri}$, $C_{s,m}$, $C_{\rm sec}$ and C_{Ia} are almost unchanged, and C_P is zero. Using the same method to study CS 22892-052([Fe/H] $= -3.10$), the coefficients are $C_{r,m} = 50.44$, $C_{\rm pri} = 2.74$ and $C_p = 0.21$ (Li et al. 2013). Comparing the coefficient C_p of HD 222925 with that of CS 22892-052, we can see that there is no Prompt component contribution to the abundances of HD 222925, which is consistent with the conclusion of Li et al. (2013), i.e., the contribution of Prompt component would be invisible for higher metallicities.

The best fit between the calculated and observed abundances of HD 222925 is shown in Figure 1. In the top panel, the calculated and the observed abundances are represented by the solid line and filled red circles. In the bottom panel, the relative offsets ($\triangle \log \epsilon = \log N_{i,\rm obs} - \log N_{i,\rm cal}$) with the observed uncertainties are shown. In Figure 1, the elements with the upper limits on the abundances (eg. Li, Be, B, Rb, Ta, Bi and U) are marked with triangles, and the elements P, S and K that are not fitted are also marked with diamonds. From Figure 1, it can be found that, whether the light elements, the iron group elements or the neutron-capture elements, most of their calculated abundances are consistent with the observed ones within the uncertainties. We can also find that the deviation of Ga is slightly large. The Ga abundance was measured using the Ga II line at 2090.768 Å, but excess absorption of 20% continuous depth is found at this wavelength in the spectrum of HD 222925 (Roederer et al. 2022), which affects the adopted abundance of Ga. Further, we speculate that the larger deviation of Cd can be due to the fact that Cd in HD 222925 does not meet well the linear relationship between the relative contribution of the weak *r*-process to the *r*-process abundances and the atomic number.

In addition, we calculate the component abundances of the main *r*-, primary, main *s*- and secondary processes, respectively. The comparison between the component abundances and the observed abundances of HD 222925 is presented in Figure 2.

In the multiple components model, the value of χ^2 is mainly influenced by the errors of the observed abundances and the error in the model itself. According to Equation (2), when the parameter K is large, the value of χ^2 can be used to describe the comparison of the relative offsets ($\triangle \log \epsilon = \log N_{i,\rm obs} - \log N_{i,\rm cal}$) and the observed errors ($\triangle \log N_{i,\rm obs}$). If the value of χ^2 is 1, the relative offsets are approximately equal to the observation errors, which means that the calculated abundances of elements are within the errors of the observed abundances. Our χ^2 value of 1.71 indicates that the relative

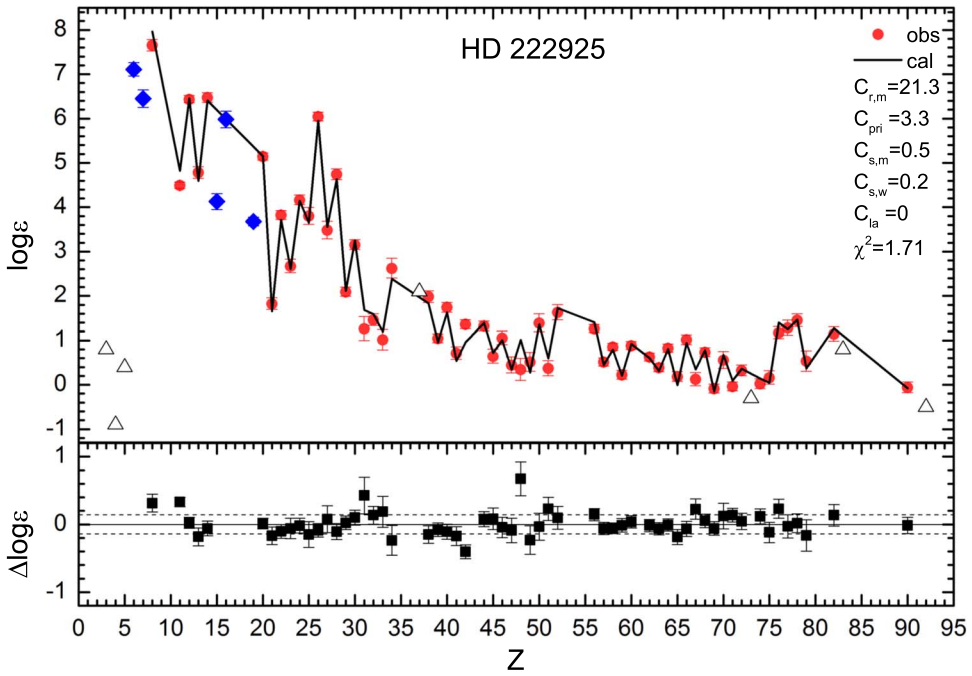

Figure 1. Top panel: The best fit of the calculated abundances of 58 elements in HD 222925 (the solid line) and the observed abundances (filled red circles). The observed upper limits are marked by triangles, and elements not fitted are also marked by diamonds. Bottom panel: the relative offsets ($\triangle \log \epsilon = \log N_{i,\mathrm{obs}} - \log N_{i,\mathrm{cal}}$) and the observed uncertainties.

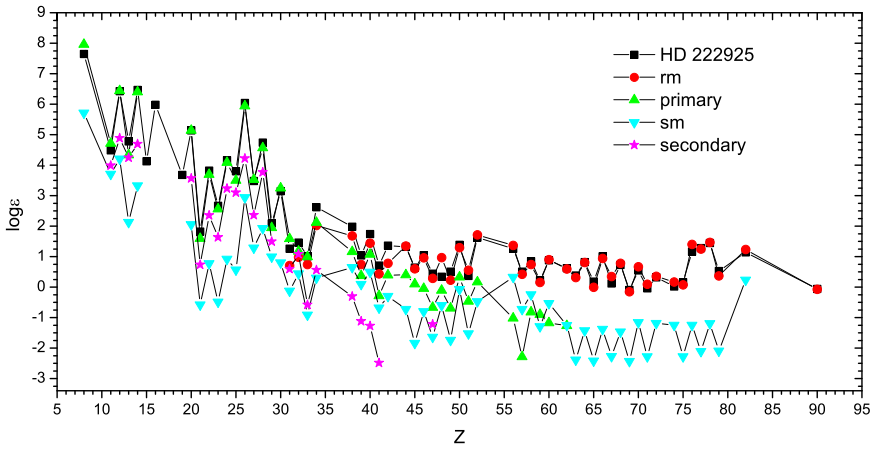

Figure 2. Comparisons between the component abundances of the main *r*-, primary, main *s*- and secondary processes and the observed abundances of HD 222925.

offsets are 1.3 times as large as the observation errors. The larger χ^2 value we obtain is mainly related to two elements, Ga and Cd, which do not fit well in Figure 1. If we remove these two elements and refit, the χ^2 value can be reduced to 1.42.

3.2. The Astrophysical Origins of Elements in HD 222925

In order to explore the astrophysical origin of elements in HD 222925, we determine the abundances ratios and components ratios of the sample star. The comparison between the observed abundances ratios, the calculated abundances ratios and components ratios of HD 222925 is presented in Figure 3. We can see that the contribution of the main *s*- and the secondary processes to the abundances of elements in HD 222925 is negligible. Further, it is clear in Figure 3 that the light and iron group elements are only associated with the primary process, while the heavy neutron-capture elements ($Z > 56$) are dominated by the main *r*-process. It indicates that

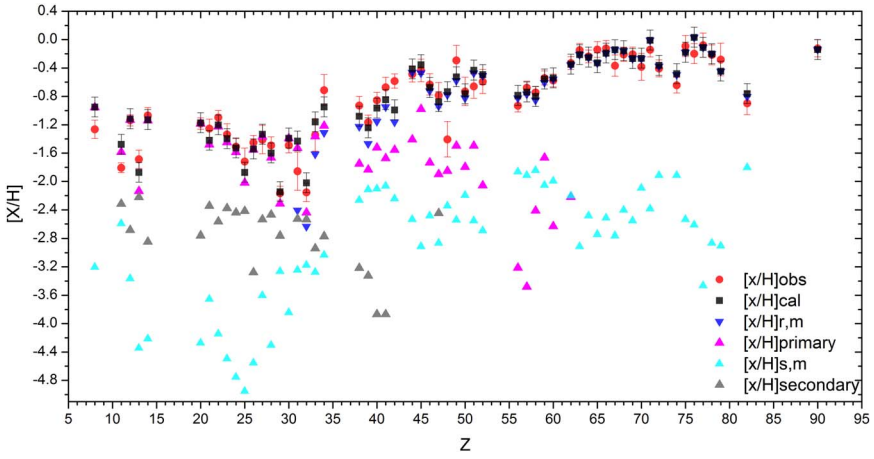

Figure 3. The observed abundances ratios, the calculated abundances ratios and components ratios of HD 222925. The components ratios include the ratios of main *r*-, primary, main *s*- and secondary components, respectively.

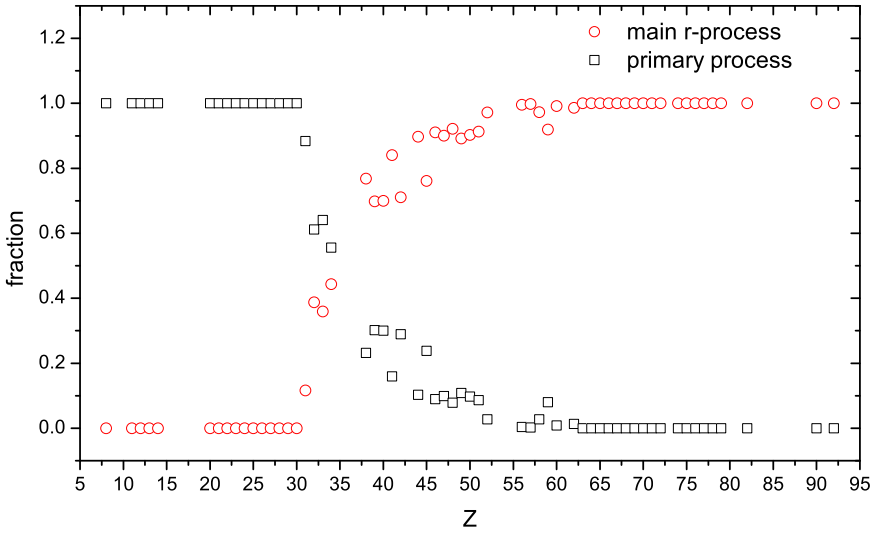

Figure 4. The relative contribution ratios of main *r*- and primary processes to elements in HD 222925. The black open rectangles are the ratios of the primary process contribution to elements and the contribution ratios of the main *r*-process are shown as red circles.

the astrophysical sites where the light elements and iron group elements are produced are different from the ones where the main *r*-process.

From Figure 3, we can find that the weak *r*-process contributes to both the light neutron-capture elements ($31 \leqslant Z \leqslant 52$) and some of the heavy neutron-capture elements ($56 \leqslant Z \leqslant 62$), but its contribution to the heavy neutron-capture elements is negligible. The relative contribution ratios of the main *r*-process to neutron capture elements are calculated as:

$$f_{i,m,r} = \frac{C_{r,m}N_{i,r,m}}{C_{r,m}N_{i,r,m} + C_{\rm pri}N_{i,\rm pri}} \quad (3)$$

where the meaning of $N_{i,r,m}$, $N_{i,\rm pri}$, $C_{r,m}$ and $C_{\rm pri}$ is the same as in Equation (1), and the values of $C_{r,m}$ and $C_{\rm pri}$ are 21.3 and 3.3. The calculated results are shown in Figure 4.

As can be seen in Figure 4, the main *r*-process does not contribute to the light elements and iron group elements in HD 222925. The contribution ratios of weak *r*-process to light neutron capture elements, e.g., Ga, Ge, As and Se, are very high and they are 0.88, 0.61, 0.64 and 0.56, respectively. Niu et al. (2014) suggested that the *r*-process is not the only way to produce Ge in the solar system and Ge can also be generated by the weak *s*-process, which can be found in Figure 3. According to the results in Section 3.1, the contribution ratio of the weak

r-process to the element Ge in HD 222925 is about 0.41, while 33% of Ge is produced by the weak *s*-process. From Figure 3, we speculate that a similar situation is likely to occur with the element Ga. The ratio of the contribution to Ga of the weak *r*- and weak *s*- processes are 0.81 and 0.08. In addition, we can also see in Figure 4 that the contribution ratios of weak *r*-process to Sr, Y, Zr, Mo and Rh are in the range of 0.23-0.30, while the ratios of contribution to Nb, Ru, Pd, Ag, Cd, In, Sn and Sb are around 0.10. The contribution of the main *r*-process is dominant in the neutron-capture elements ($Z \geqslant 38$).

3.3. Uncertainties of Component Coefficients of HD 222925

Five component coefficients that are determined in this study based on the observed abundance of HD 222925 should be subject to observation errors. We estimate the component coefficient uncertainties using $C_{r,m}$ and $C_{\rm pri}$ as examples. Since the coefficients $C_{r,m}$ and $C_{\rm pri}$ are sensitive to Eu and O abundances, respectively, the uncertainties of the two coefficients can be calculated by Eu and O abundances. Following the component coefficients $C_{\rm pri} = 3.3$, $C_{s,m} = 0.5$, $C_{\rm sec} = 0.2$ and $C_{Ia} = 0$, we obtain the variations of the abundance ratio [Eu/H] and reduced χ^2 with $C_{r,m}$, which is presented in Figure 5(a). It is found in Figure 5(a) that the calculated values of [Eu/H] lie within the range of observed ratios when $C_{r,m}$ is taken from 17.0 to 26.8. Employing the same calculation method, we also derive the variations of the abundance ratio [O/H] and reduced χ^2 with $C_{\rm pri}$, which is shown in Figure 5(b). From Figure 5(b), we see that the observed ratio [O/H] can be explained when $C_{\rm pri}$ is in the range of 2.5-4.5. In a similar way, the range of other component coefficients can be calculated: $0 < C_{s,m} < 2.0$ and $0 < C_{\rm sec} < 0.4$ for HD 222925.

4. Analysis on the Formation of HD 222925

There is one *r*-II star in the UMi dwarf system, COS 82([Fe/H] $= -1.42$, [Eu/H] $= -0.18$), whose metallicity and Eu abundance are similar to those of HD 222925. However, the ratio of α-elements to Fe in HD 222925 is about 0.40, while this ratio in COS 82 is about 0.04 (Aoki et al. 2007). The difference in the ratio of α-elements to Fe suggests that HD 222925 and COS 82 have different histories of elemental enrichment. The lower abundances of α-elements in COS 82 should be caused by the contamination with SNe Ia. There is a longer chemical enrichment timescale in dwarf galaxies, so the high Eu abundance of COS 82 may be due to the influence of multiple *r*-process events (Tsujimoto et al. 2017). From the previous calculations(see Section 3), we suggest that the light elements and iron group elements in HD 222925 come from SNe II with a progenitor mass $M > 10\,M_{\odot}$, which means that HD 222925 is unlikely to undergo multiple *r*-process events.

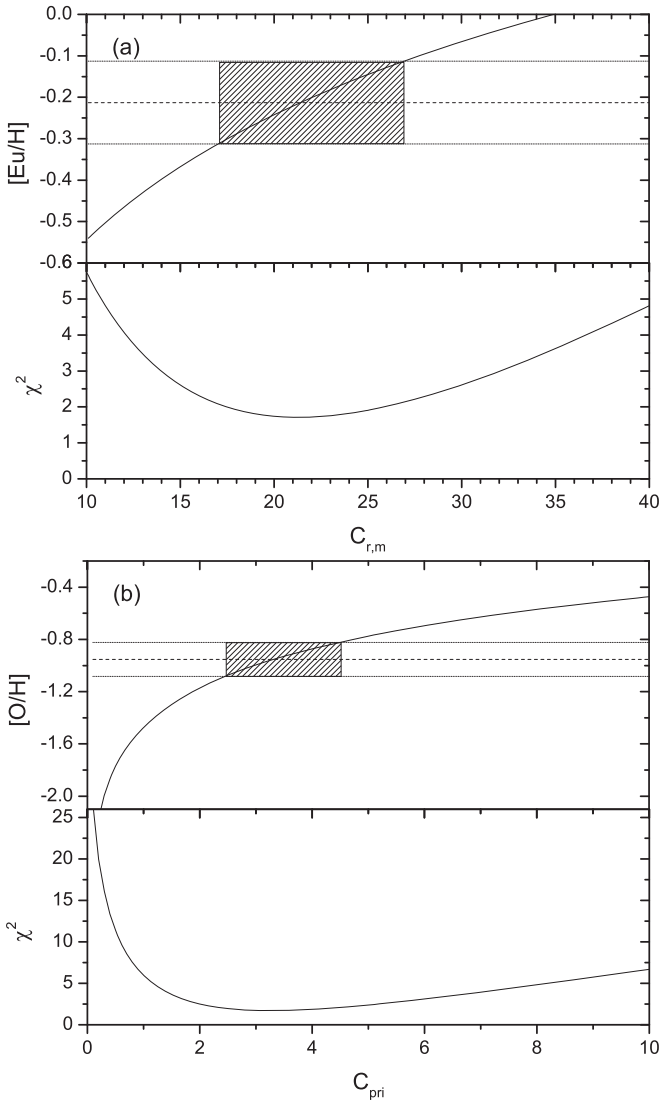

Figure 5. (a) Variation of the calculated abundance ratio [Eu/H] (upper panel) and χ^2 (lower panel) as a function of $C_{r,m}$. (b) Variation of the calculated abundance ratio [O/H] (upper panel) and χ^2 (lower panel) as a function of $C_{\rm pri}$. The calculated results are shown with solid lines. The observed values and the observed uncertainties are shown as dashed lines and dotted lines respectively. The shaded regions present the allowed ranges of the component coefficients $C_{r,m}$ and $C_{\rm pri}$.

4.1. Comparison of the Abundance Patterns between HD 222925 and Two Typical r*-II Stars*

The star CS 22892-052 is a typical *r*-II star in the Milky Way halo, and the star J033457-540531 ([Fe/H] $= -2.08$) is a moderately metal-poor *r*-II star in the ultra-faint dwarf galaxy Ret II with [Eu/H] $= -0.31$ (Ji et al. 2016). We compare the abundance pattern of HD 222925 with that of CS 22892-052 and J033457-540531 (see Figure 6). The element abundances

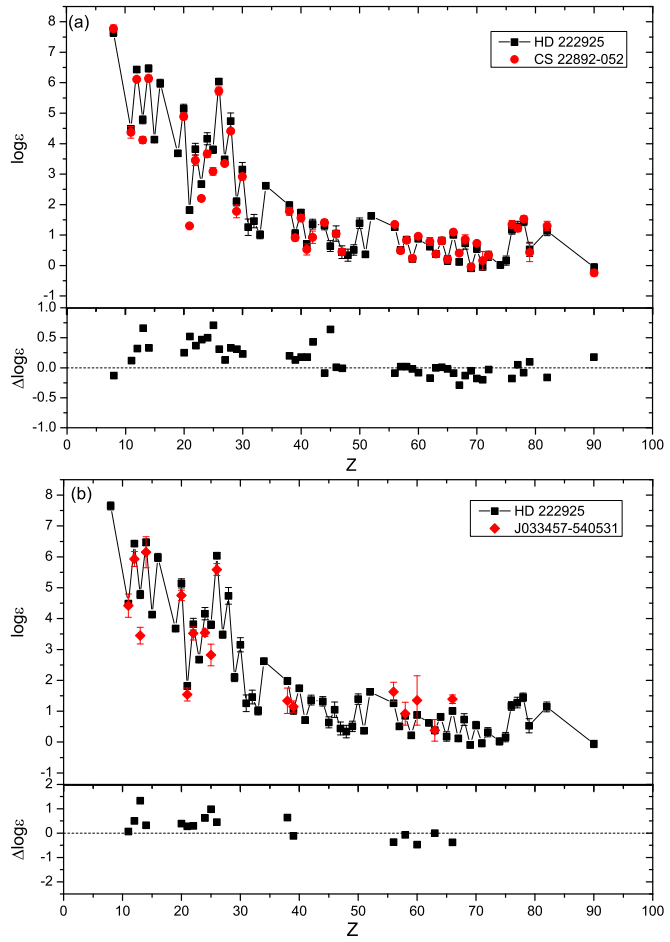

Figure 6. Top panel: comparison of the elemental pattern of HD 222925 against the abundance patterns of CS22892-052 and J033457-540531. The observed abundances of the sample stars are shown as black rectangles, while those of CS22892-052 and J033457-540531 are shown as red circles and diamonds, respectively. Bottom panel: the relative offsets ($\triangle \log \epsilon = \log \epsilon_{\rm HD\ 222925} - \log \epsilon_{\rm CS22892-052\ or\ J033457-540531}$).

of two stars have been normalized to the Eu abundance of HD 222925, respectively.

From Figure 6, the larger deviations are presented for the light element comparison of HD 222925 with CS 22892-052 and J033457-540531, but the deviations among neutron-capture elements with $Z > 56$ are relatively small, which suggests that the main *r*-process is mostly independent of the environment of the star (Johnson et al. 2013). By comparing the observed and theoretical abundances of CS 22892-052, Ramirez-Ruiz et al. (2015) suggested that the *r*-process elements in this star originate from a single *r*-process event: NSM. Ji et al. (2016) noted that Ret II had undergone a single rare *r*-process event that had resulted in a 2–3 magnitude higher abundance of heavy neutron-capture elements in *r*-II stars in this galaxy than in other ultra-faint dwarf galaxies, and they speculated that this single *r*-process event is an NSM. Considering the fact that the Eu abundance ([Eu/H] = −0.14) of HD 222925 is much higher than those of CS 22892-052 and J033457-540531, we infer that this star was affected by a single, high-yield *r*-process. Roederer et al. (2018) explained the observed [Eu/H] ratio of HD 222925 due to the *r*-process material ejected by an NSM. We therefore speculate that the *r*-process event affecting HD222925 is most likely to be an NSM.

Combined with the analysis in Section 3, we hypothesize that HD 222925 is likely to be first contaminated by a Type II supernova with the progenitor mass $M > 10 M_{\odot}$, which increased its Fe abundance, and then by a high-yield NSM, which enriched the *r*-process elements. Our view is consistent with that of Roederer et al. (2018, 2022).

4.2. Explanation of the Observed Abundance of Eu in HD 222925

Komiya & Shigeyama (2016) indicated that the mass of an NSM ejecting Eu is about $1.5 \times 10^{-4} M_{\odot}$ and the mass of the cloud contaminated by a single main *r*-process is about $10^{7} M_{\odot}$ based on the study of the [r/Fe] scatter of metal-poor stars. We assume that the environment in which HD 222925 was born is consistent with the conclusion of Komiya & Shigeyama (2016), and using the method of calculation in Yang et al. (2017), the Eu abundance of HD 222925 can be calculated according to the following equation:

$$\frac{N_{\rm Eu}}{N_{\rm Fe}} = \left(\frac{A_{\rm Fe}}{A_{\rm Eu}}\right) \frac{M_{\rm SW} X_{\rm Eu} + Y_{\rm Eu}}{M_{\rm SW} X_{\rm Fe}} \quad (4)$$

where $M_{\rm SW}$ is the mass of the cloud where the star was born. $X_{\rm Eu}$ and $X_{\rm Fe}$ are the initial mass fractions of Eu and Fe in the cloud. $Y_{\rm Eu}$ is the mass of Eu elements ejected by the main *r*-process event. $A_{\rm Eu}$ and $A_{\rm Fe}$ are the atomic weights of Eu and Fe, respectively. The mean value of [Eu/Fe] in Cescutti et al. (2006) is used as the initial Eu abundance of the cloud. We adopt the data in Komiya & Shigeyama (2016), then the calculated Eu abundance of HD 222925 is about 0.60, which is not consistent with the observed Eu abundance ([Eu/Fe] = 1.32). There are three possible scenarios that cause the calculated Eu abundance of HD 222925 to be much lower than the observed abundance, and they are as follows: (1) If HD 222925 was born in a cloud of mass $10^{7} M_{\odot}$, then the yield of Eu ejected by an NSM should be larger than $1.5 \times 10^{-4} M_{\odot}$. (2) If the yield of Eu ejected by the NSM is $1.5 \times 10^{-4} M_{\odot}$, then the mass of the contaminated cloud should be less than $10^{7} M_{\odot}$. (3) Both the yield of Eu ejected by an NSM and the mass of the cloud where HD 222925 was born differ from the results in Komiya & Shigeyama (2016).

To be able to interpret the observed abundance of Eu in HD 222925, we discuss the following three scenarios. As a comparison, CS 22892-052 also is discussed accordingly and the results of the calculations are also shown in the figure. The

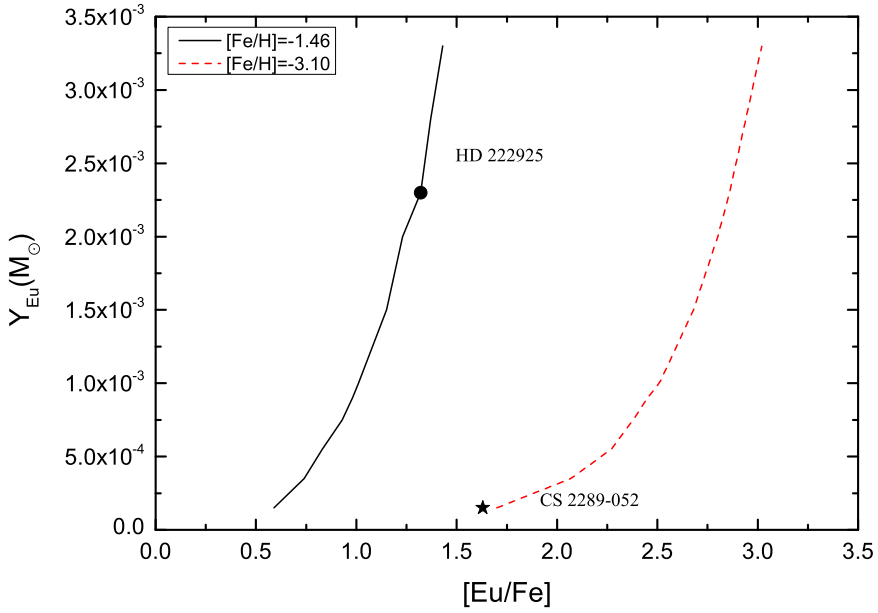

Figure 7. The trend of the yield of Eu ejected by an NSM with [Eu/Fe] for a cloud mass of $10^7 M_\odot$ and metal abundances of –1.46 (black solid line) and –3.10 (red dashed line). HD 222925 and CS 22892-052 are marked with a dot and a pentagram, respectively.

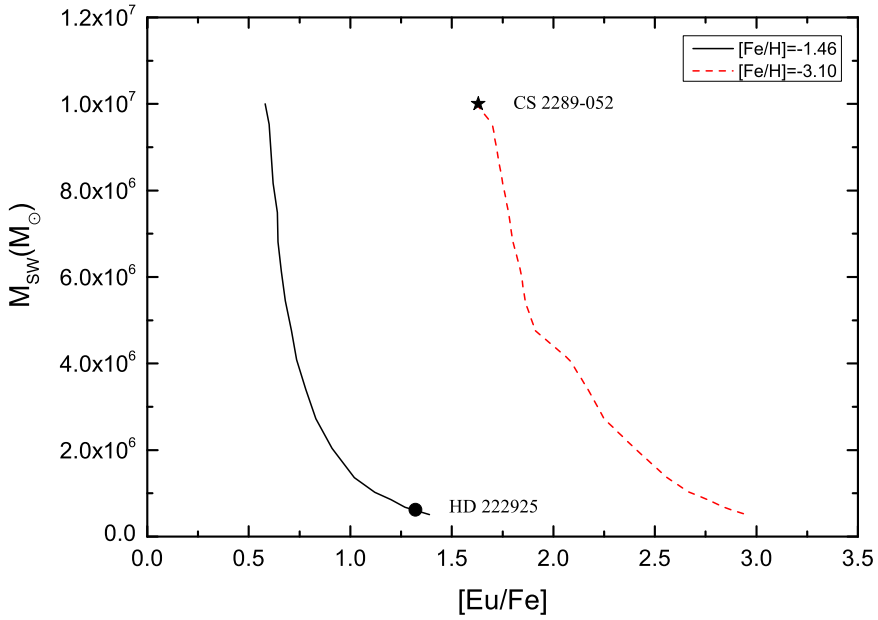

Figure 8. The trend of the cloud mass with [Eu/Fe] for the yield of Eu ejected by an NSM of $1.5 \times 10^{-4} M_\odot$ and metal abundances of –1.46 (black solid line) and –3.10 (red dashed line). HD 222925 and CS 22892-052 are marked with a dot and a pentagram, respectively.

first scenario is as follows: (1) Fixing the cloud mass ($10^7 M_\odot$) and stellar metal abundances([Fe/H] = −1.46 and −3.10]), the variation of the yield of Eu ejected by an NSM with Eu abundance is discussed (see Figure 7). It is found in Figure 7 that the required yield of Eu ejected by an NSM increases rapidly as the Eu abundance increases at a fixed cloud mass and at two metal abundances. For [Fe/H] = −1.46, when the yield of Eu ejected by an NSM is 0.0023 $M_\odot$, the Eu abundance is about 1.32, which is consistent with the observed abundance of HD 222925. It means that if HD 222925 was born in a cloud of mass $10^7 M_\odot$, then an Eu yield of 0.0023 $M_\odot$ is sufficient to achieve the observed abundance of Eu in HD 222925.

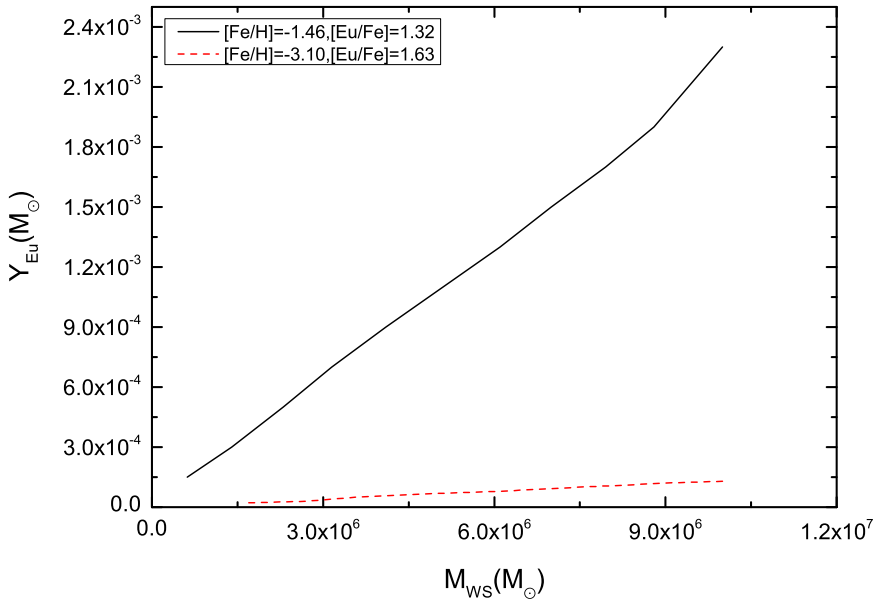

Figure 9. Variation of the Eu yield from an NSM with the cloud mass for fixed metal and Eu abundances. [Fe/H] = −1.46 and [Fe/H] = −3.10 correspond to the black solid line and the dashed red line, respectively.

The second scenario is as follows: (2) Fixing the yield of Eu ejected by an NSM ($1.5 \times 10^{-4} M_{\odot}$) and stellar metal abundances([Fe/H] = −1.46 and −3.10), the variation of the cloud mass with Eu abundance is discussed (see Figure 8). We can see that the cloud mass decreases rapidly with increasing Eu abundance at a fixed yield of Eu and at two metal abundances. For [Fe/H] = −1.46, if HD 222925 was born in a cloud of mass $6.2 \times 10^{5} M_{\odot}$, then its observed abundance of Eu can be explained.

The third scenario is as follows: (3) Fixing stellar metal abundances([Fe/H] = −1.46 and −3.10) and Eu abundances ([Eu/Fe] = 1.32 and 1.63), the relationship between the cloud mass and the yield of Eu ejected by an NSM is discussed (see Figure 9). As can be seen from Figure 9, the Eu yield increases linearly with increasing the cloud mass for both abundance cases, which is consistent with equations (5). However, we note that for [Fe/H] = −1.46, the Eu yield increases rapidly with increasing the cloud mass, while for [Fe/H] = −3.10, the Eu yield increases more slowly, which is mainly due to the different metal abundances.

5. Conclusion

The *r*-II stars can provide us with useful information to investigate the astrophysical origin and the yield of the *r*-process, and so on. In this paper, we use the five component model to study the elemental abundances and explore the possible astrophysical origins of the elements in the *r*-II star HD 222925. In addition, adopting the conclusions of Komiya & Shigeyama (2016) and the method of Yang et al. (2017), we investigate the relationship between the mass of the molecular cloud where HD 222925 was born and the yield of Eu ejected by an NSM. We conclude the following points:

(1) The component coefficients, $C_{r,m} = 21.3$, $C_{r,\mathrm{pri}} = 3.3$, $C_{s,m} = 0.5$, $C_{\mathrm{sec}} = 0.2$, $C_{Ia} = 0$ and $C_{p} = 0$, are derived, which suggest that the *s*-process has very little effect on the *r*-II star HD 222925 and SNe Ia does not contribute to its elemental abundances. we also find no contribution of the first generation of very massive stars to the abundances of HD 222925, which confirms the prediction by Li et al. (2013) that the contribution of Prompt component may be not present at higher metallicities.

(2) The light elements and the iron group elements in HD 222925 are mainly from the primary process of Type II supernova with a progenitor mass $M > 10 M_{\odot}$. A fraction of the light neutron-capture elements ($31 \leqslant Z \leqslant 52$) in HD 222925 originates from weak *r*-process, while another fraction originates from main *r*-process, and the contribution of main *r*-process increases linearly with increasing atomic number, which is consistent with the conclusions of Li et al. (2013). The heavy neutron-capture elements ($Z \geqslant 38$) in HD 222925 dominantly come from the main *r*-process.

(3) We deduce that HD 222925 is likely to be contaminated by an NSM, which causes a significant enhancement of Eu in HD 222925. We find that if HD 222925 was born in a molecular cloud of mass $10^{7} M_{\odot}$, the Eu yield of $0.0023 M_{\odot}$ ejected by an NSM is sufficient to achieve the observed abundance of Eu in HD 222925. In the other case, if the yield of Eu ejected by an NSM is $1.5 \times 10^{-4} M_{\odot}$, the observed abundance of Eu in HD 222925 can be interpreted for a

molecular cloud with a mass of $6.2 \times 10^5 M_{\odot}$. Our opinions are in agreement with those of Roederer et al. (2018, 2022).

Acknowledgments

This work was supported by the National Natural Science Foundation of China (NSFC) under grants 12 173 013, 11 773 009, the National Key Basic R&D Program of China via 2019YFA0405500. W.Y.C. is supported by the "333 talents project" of Hebei Province under the number A202010001. This work is also supported by the Natural Science Foundation of Hebei Province under grant A2021205006, by the project of the Hebei provincial department of science and technology under grant number 226Z7604G, and by Scientific Research Project of Hebei Province (ZC2022090) and Shijiazhuang University Doctoral Scientific Research Fund Project (21BS014).

References

Abbott, B. P., Abbott, R., Abbott, T. D., et al. 2017, PhRvL, 119, 161101
Aoki, W., Honda, S., Sadakane, K., & Arimoto, N. 2007, PASJ, 59, L15
Arlandini, C., Käppeler, F., Wisshak, K., et al. 1999, ApJ, 525, 886
Barklem, P. S., Christlieb, N., Beers, T. C., et al. 2005, A&A, 439, 129
Beers, T. C., & Christlieb, N. 2005, ARA&A, 43, 531
Bisterzo, S., Gallino, R., Straniero, O., Cristallo, S., & Käppeler, F. 2010, MNRAS, 404, 1529
Buridge, E. M., & Burbidge, G. R. 1957, ApJ, 126, 357
Burris, D. L., Pilachowski, C. A., Armandroff, T. E., et al. 2000, ApJ, 544, 302
Cayrel, R., Hill, V., Beers, T. C., et al. 2001, Natur, 409, 691
Cescutti, G., François, P., Matteucci, F., Cayrel, R., & Spite, M. 2006, A&A, 448, 557
Cohen, J. G., & Huang, W. 2009, ApJ, 701, 1053
Dvorkin, I., Daigne, F., Goriely, S., Vangioni, E., & Silk, J. 2021, MNRAS, 506, 4374
Fraser, J., & Schönrich, R. 2022, MNRAS, 509, 6008
Frebel, A. 2010, AN, 331, 474
Frebel, A., Christlieb, N., Norris, J. E., et al. 2007, ApJL, 660, L117
Freiburghaus, C., Rosswog, S., & Thielemann, F. K. 1999, ApJL, 525, L121
Goriely, S. 2012, in AIP Conf. Ser. 1491, Nuclear Structure and Dynamics 2012, ed. T. Nikšić et al. (Melville, NY: AIP), 263
Gratton, R. G., Sneden, C., Carretta, E., & Bragaglia, A. 2000, A&A, 354, 169
Han, W., Zhang, L., Yang, G., Niu, P., & Zhang, B. 2018, ApJ, 856, 58
Han, W.-Q., Zhang, L., Yang, G.-C., et al. 2020, RAA, 20, 059
Hansen, T. T., Holmbeck, E. M., Beers, T. C., et al. 2018, ApJ, 858, 92
Hayek, W., Wiesendahl, U., Christlieb, N., et al. 2009, A&A, 504, 511
Ivans, I. I., Simmerer, J., Sneden, C., et al. 2006, ApJ, 645, 613
Ji, A. P., Frebel, A., Simon, J. D., & Chiti, A. 2016, ApJ, 830, 93
Johnson, C. I., McWilliam, A., & Rich, R. M. 2013, ApJL, 775, L27
Kelson, D. D. 2003, PASP, 115, 688
Kelson, D. D., Illingworth, G. D., van Dokkum, P. G., & Franx, M. 2000, ApJ, 531, 159
Kobayashi, C., Tsujimoto, T., Nomoto, K., Hachisu, I., & Kato, M. 1998, ApJL, 503, L155
Komiya, Y., & Shigeyama, T. 2016, ApJ, 830, 76
Letarte, B., Hill, V., Tolstoy, E., et al. 2010, A&A, 523, A17
Li, H., Shen, X., Liang, S., Cui, W., & Zhang, B. 2013, PASP, 125, 143
Li, H.-N., Aoki, W., Honda, S., et al. 2015, RAA, 15, 1264
MacFadyen, A. I., & Woosley, S. E. 1999, ApJ, 524, 262
Mösta, P., Roberts, L. F., Halevi, G., et al. 2018, ApJ, 864, 171
Navarrete, C., Chanamé, J., Ramírez, I., et al. 2015, ApJ, 808, 103
Nishimura, N., Takiwaki, T., & Thielemann, F.-K. 2015, ApJ, 810, 109
Niu, P., Liu, W., Cui, W., & Zhang, B. 2014, MNRAS, 443, 2426
Qian, Y. Z., & Wasserburg, G. J. 2001, ApJ, 559, 925
Ramirez-Ruiz, E., Trenti, M., MacLeod, M., et al. 2015, ApJL, 802, L22
Roederer, I. U., Lawler, J. E., Den Hartog, E. A., et al. 2022, ApJS, 260, 27
Roederer, I. U., Sakari, C. M., Placco, V. M., et al. 2018, ApJ, 865, 129
Roederer, I. U., Sneden, C., Lawler, J. E., & Cowan, J. J. 2010, ApJL, 714, L123
Shetrone, M. D., Côté, P., & Sargent, W. L. W. 2001, ApJ, 548, 592
Sneden, C., McWilliam, A., Preston, G. W., et al. 1996, ApJ, 467, 819
Travaglio, C., Gallino, R., Arnone, E., et al. 2004, ApJ, 601, 864
Tsujimoto, T. 2011, ApJ, 736, 113
Tsujimoto, T., Matsuno, T., Aoki, W., Ishigaki, M. N., & Shigeyama, T. 2017, ApJL, 850, L12
Watson, D., Hansen, C. J., Selsing, J., et al. 2019, Natur, 574, 497
Winteler, C., Käppeli, R., Perego, A., et al. 2012, ApJL, 750, L22
Woosley, S. E., & Weaver, T. A. 1995, ApJS, 101, 181
Yang, G., Li, H., Liu, N., et al. 2017, PASP, 129, 064201